Abdominal Radiology (2023) 48:3101–3113
https://doi.org/10.1007/s00261-023-03993-z

HEPATOBILIARY

Nomogram based on Sonazoid contrast-enhanced ultrasound to differentiate intrahepatic cholangiocarcinoma and poorly differentiated hepatocellular carcinoma: a prospective multicenter study

Shuo Wang · Jundong Yao · Kaiyan Li · Hong Yang · Shichun Lu · Guangzhi He, et al. ***[full author details at the end of the article]***

Received: 3 April 2023 / Revised: 17 June 2023 / Accepted: 18 June 2023 / Published online: 12 July 2023

Abstract

Objectives The aim of this study was to develop a predictive model based on Sonazoid contrast-enhanced ultrasound (SCEUS) and clinical features to discriminate poorly differentiated hepatocellular carcinoma (P-HCC) from intrahepatic cholangiocarcinoma (ICC).

Patients and method Forty-one ICC and forty-nine P-HCC patients were enrolled in this study. The CEUS LI-RADS category was assigned according to CEUS LI-RADS version 2017. Based on SCEUS and clinical features, a predicated model was established. Multivariate logistic regression analysis and LASSO logistic regression were used to identify the most valuable features, 400 times repeated 3-fold cross-validation was performed on the nomogram model and the model performance was determined by its discrimination, calibration, and clinical usefulness.

Results Multivariate logistic regression and LASSO logistic regression indicated that age (> 51 y), viral hepatitis (No), AFP level (≤ 20 μg/L), washout time (≤ 45 s), and enhancement level in the Kupffer phase (Defect) were valuable predictors related to ICC. The area under the receiver operating characteristic (AUC) of the nomogram was 0.930 (95% CI: 0.856–0.973), much higher than the subjective assessment by the sonographers and CEUS LI-RADS categories. The calibration curve showed that the predicted incidence was more consistent with the actual incidence of ICC, and 400 times repeated 3-fold cross-validation revealed good discrimination with a mean AUC of 0.851. Decision curve analysis showed that the nomogram could increase the net benefit for patients.

Conclusions The nomogram based on SCEUS and clinical features can effectively differentiate P-HCC from ICC

Graphical abstract

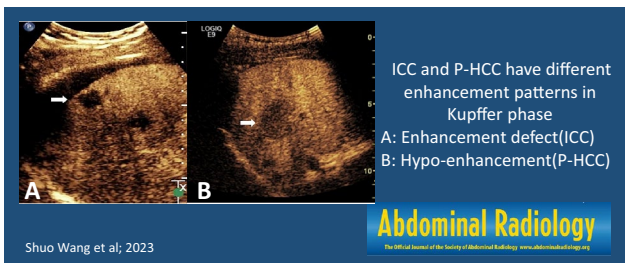

Keywords Sonazoid contrast-enhanced ultrasound · Poorly differentiated hepatocellular carcinoma · Intrahepatic cholangiocarcinoma · Nomogram

Shuo Wang and Jundong Yao have contributed equally to this work.

Abbreviations

AP	Arterial phase
AUC	Area under the receiver operating characteristic

CEUS	Contrast-enhanced ultrasound
CI	Confidence interval
HCC	Hepatocellular carcinoma
ICC	Intrahepatic cholangiocarcinoma
KP	Kupffer phase
OR	Odds ratio
P-HCC	Poorly differentiated hepatocellular carcinoma
ROI	Region of interest
SCEUS	Sonazoid contrast-enhanced ultrasound

Introduction

Primary liver cancer, including hepatocellular carcinoma (HCC), intrahepatic cholangiocarcinoma (ICC), and other types, has become the sixth most prevalent cancer and the third leading cause of cancer-related death worldwide [1, 2]. HCC is the most common primary liver cancer and may be cured by a variety of treatment modalities (liver resection, liver transplantation, local ablation, etc.) [3, 4]. Unfortunately, the prognosis of ICC is significantly worse than that of HCC, with radical surgery being the only curative treatment, and extended hepatectomy is required [5, 6]. The treatment strategies and prognosis between HCC and ICC are significantly different, and accurate noninvasive preoperative diagnosis is essential [7].

Contrast-enhanced ultrasound (CEUS) has been widely used for noninvasive diagnosis before treatment. Typical features of CEUS in ICC include rim enhancement, early washout time (< 60 seconds), and marked washout [8]. However, the presence of early washout time in some poorly differentiated hepatocellular carcinomas (P-HCCs) can lead to overlapping CEUS features of P-HCC and ICC, thereby making accurate identification challenging [9, 10].

In recent years, Sonazoid® has been launched in some countries as a contrast agent with some differences from other contrast agents. One characteristic of Sonazoid® is its unique Kupffer phase (KP), which enables continuous scanning without microbubbles being destroyed [2, 11]. Sugimoto K, et al. [12] demonstrated that the perfusion performance in KP was closely related to the pathological grade of HCC, suggesting that KP perfusion may serve as an independent and effective predictor for differentiating between well-differentiated HCC, moderately differentiated HCC, or P-HCC [13, 14].

There are few reports on the preoperative diagnosis of ICC and P-HCC by Sonazoid contrast-enhanced ultrasound (SCEUS). Therefore, we aimed to develop a nomogram using SCEUS and clinical features to improve diagnostic accuracy in distinguishing between ICC and P-HCC.

Material and methods

Study population

Using data from a prospective, multicenter study designed for sample collection (Clinical Trials.gov identifier: NCT04563897), we retrospectively analyzed SCEUS scans and clinical data from a total of 90 adults who were diagnosed with ICC and P-HCC. This study included 16 medical institutions (Supplement Table 1) and was approved by the Institutional Review Boards at each center (S2020-300-01). All participants provided written informed consent. The research protocol, which included the eligibility criteria and standardized data access procedures, was implemented consistently across all participating institutions. The flowchart of the study population selection process is shown in Fig. 1.

Clinicopathologic information

Clinical data were collected, including age, sex, and serum markers. The target lesions were diagnosed histopathologically (surgery, n = 26; biopsy, n = 64). Histological diagnosis was made by at least two experienced pathologists according to the World Health Organization criteria [15].

Sonazoid contrast-enhanced ultrasound

Gray-scale ultrasound and contrast-enhanced ultrasound were performed in medical institutions using ultrasound equipment with contrast-enhancing software (GE Healthcare, Philips, Siemens, Mindray). The abdominal probe (frequency 2-6 MHz) was used, and the mechanical index ranged from 0.16 to 0.21. The second-generation contrast agent Sonazoid (GE Healthcare AS, Oslo, Norway), a lipid-encapsulated perfluorobutane microbubble, was injected at a dose of 0.015 ml/kg through the antecubital vein, followed immediately by a flush of 5 mL of 0.9% normal saline solution. The largest lesion was observed continuously, and videos of arterial phases (0-30 s) and portal phases (31–120 s) were stored. After vascular phases (120 s), the first 10 s of intermittent imaging was stored every minute until 10 min or the disappearance of the liver parenchyma contrast agent (for evaluating KP) [16]. All the images were stored on hard drives for offline analysis.

Analysis of ultrasound and Sonazoid contrast-enhanced ultrasound features

Ultrasound and SCEUS images were retrospectively reviewed by two sonographers who had more than six years of experience in abdominal ultrasound imaging, independently. All lesions were assessed and classified according

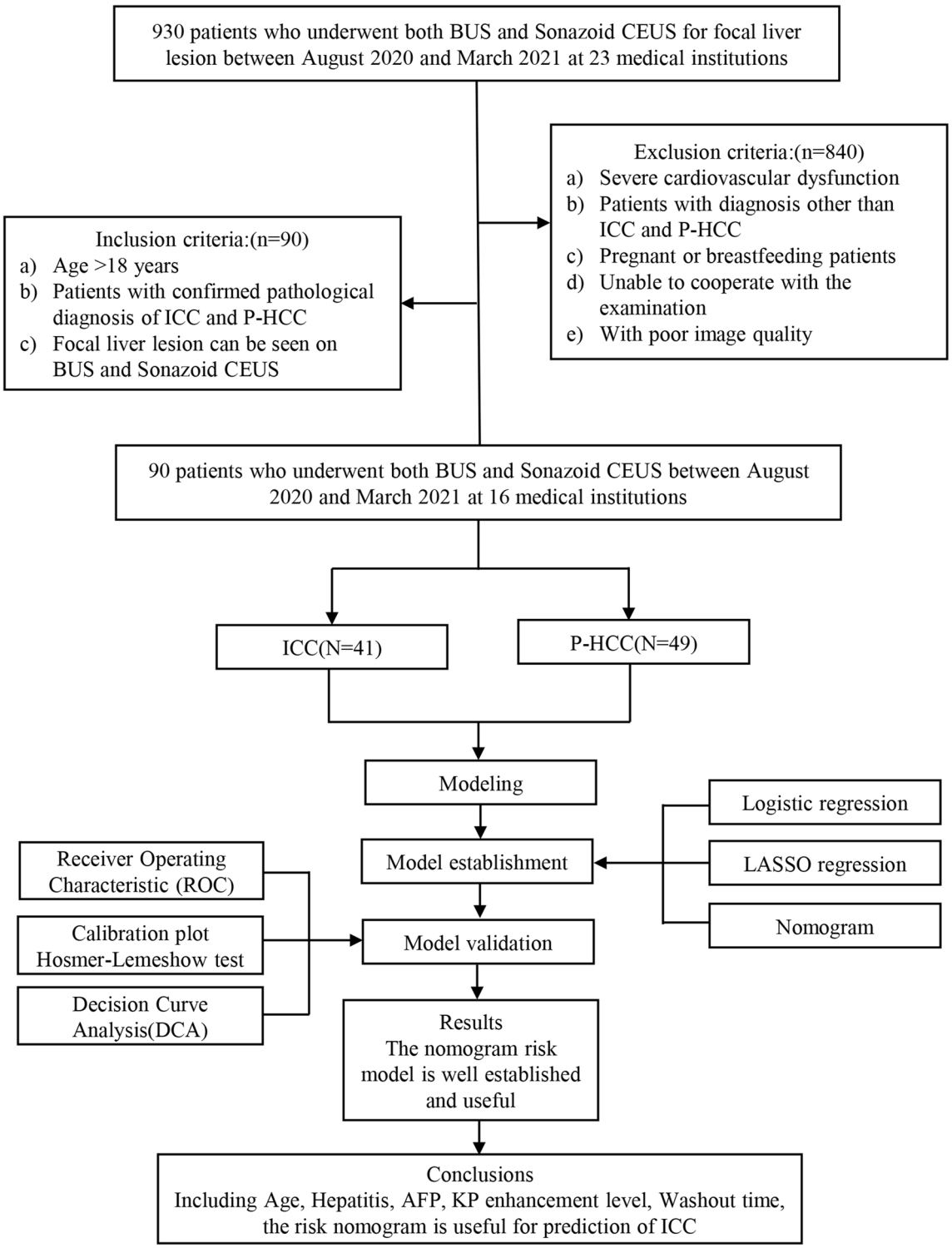

Fig. 1 Flowchart of the study population selection process

to CEUS LI-RADS version 2017 [17]. If there was any discordance, the images were rereviewed, and a consensus was reached by discussion.

The SCEUS features of the lesion were characterized as follows: (1) the echo and size (mm) of the lesion;(2) enhancement levels in the AP (hypo-enhancement /iso-enhancement /hyper-enhancement); (3) enhancement pattern in the AP(Rim enhancement and mosaic architecture [18, 19]); (4)washout time($\leq$ 45 s) [20, 21]; (5) critical features according to CEUS LI-RADS version 2017, including AP

hyper-enhancement and late and mild washout (in contrast to the liver in the portal venous phase, the lesion showed hypo-enhancement within 60 seconds of contrast injection and no apparent hypo-enhancement or contrast defect within 2 minutes of contrast injection) [16, 22]; and (6) KP hypo-enhancement (lesions with low enhancement compared to the liver in KP) or KP defect (lesions with similar non-enhancement compared to the liver in KP) [20]. If two or more lesions were present in a single patient, the histologically confirmed lesion or the largest lesion was selected as the target lesion.

Gray-scale analysis of Kupffer phase images by ImageJ

KP images were exported to a personal computer in JPEG format and analyzed using ImageJ version 1.47 software (National Institutes of Health, Bethesda, MD). Two sonographers freehand outlined the lesion, which was marked as a region of interest (ROI)1 and the surrounding liver parenchyma as ROI2. The shape, size, and depth of ROI2 are consistent with those of ROI1. Then, the ROI Manager mode was used for a gray analysis of the outlines. The mean gray value, modal gray value, minimum gray value, maximum gray value, and standard deviation of the gray value of the lesions were measured [23]. The measurement was repeated five times, and the average gray value was calculated. The average mean gray value was then used to calculate the gray value ratio (gray value ratio=average mean gray value of liver parenchyma/average mean gray value of lesion).

Development and validation of a nomogram to distinguish between ICC and P-HCC

Multivariate logistic regression and LASSO regression were used to filter variables, and a nomogram model was constructed to predict ICC. The Hosmer-Lemeshow test was used to assess the goodness of fit of the model. A receiver operating characteristic (ROC) curve, the area under the ROC curve (AUC), the concordance index (C-statistic), and the calibration curve were used to evaluate the predictive accuracy and consistency of the model. Discrimination and calibration were assessed by 1000 bootstrapping validations and internally validated by 400 times repeated 3-fold cross-validation. Decision curve analysis (DCA) reflects the model's net benefit to the patient.

Statistical analysis

All analyses were performed using IBM SPSS Statistics 26 for Windows (IBM Corp, Armonk, NY, USA) , R software (version 4.2.1), and MedCalc version 9.0 software (MedCalc Software, Mariakerke, Belgium). The differences in clinical and SCEUS features were compared between ICC and P-HCC using independent samples t -tests, chi-square tests, Fisher's exact tests, or Mann–Whitney U-tests. Inter-observer agreement of features between two sonographers was assessed using Cohen's kappa coefficients and 95% confidence intervals. Univariate and multivariate regression analyses were performed via SPSS 26.0. ICC was predicted using binary logistic regression analysis. ROC curve analysis was drawn via MedCalc. The McNemar test was used to compare the clinical usefulness of each diagnostic method. The difference was statistically significant when the two-tailed P-value was < 0.05.

Via R software, the "glmnet" package was used for LASSO regression, the "rms" package was used to plot the nomogram, the "pec" package was used to construct the calibration curves, the "caret" package was used for bootstrapping validation and k-fold cross-validation, and clinical decision curves were constructed using the "ggDCA" package.

Results

Patient characteristics

The baseline characteristics of the clinical and ultrasound images are shown in Table 1, including 41 ICC and 49 P-HCC. A total of 13 patients showed hyperechoic lesions, including 11 patients (11/13) in the P-HCC group and two patients (2/13) in the ICC group. Of the 13 hyperechoic lesions, 12 had hepatitis.

As shown in Table 2, among the SCEUS features, there were significant differences between the two groups of patients in the washout time (whether ≤ 45 s) and the enhancement level in the KP. In addition, the consistency of subjective assessment of the enhancement level in the KP between the two sonographers was high, with a kappa-value of 0.773.

Gray-scale analysis of Kupffer phase images by ImageJ

The gray-scale analysis is shown in Supplemental Table 2. The cutoff value of the mean gray value between ICC and P-HCC was 24.92, and the cutoff value of the modal gray value, minimum gray value, and gray value ratio were 10.00, 0.00, and 2.24, respectively. These values were significantly different between ICC and P-HCC ($P < 0.05$).

Table 1 Patients clinical and ultrasound features

Features	ICC (n = 41)	P-HCC (n = 49)	P
Age (years)[a]	58.00 (52.50, 64.50)	51.00 (43.50, 62.00)	0.006*
Sex			0.021*
Male	29 (70.73%)	44 (89.80%)	
Female	12 (29.27%)	5 (10.20%)	
BMI (kg/m^2)[b]	23.83±2.85	23.61±3.05	0.729
Hepatitis			< 0.001*
Yes	18 (43.90%)	44 (89.80%)	
No	23 (56.10%)	5 (10.20%)	
AFP> 20ug/L	10 (24.39%)	36 (73.47%)	< 0.001*
CA199> 37u/mL	20 (48.78%)	13 (26.53%)	0.029*
Location			0.817
Right lobe	31 (75.61%)	36 (73.47%)	
Left lobe	10 (24.39%)	13 (26.53%)	
Tumor size (mm)[b]	60.64±32.30	53.74±29.51	0.293
Gray-scale echogenicity			0.038*
Hypoechoic	34 (82.93%)	30 (61.22%)	
Un-hypoechoic	7 (17.07%)	19 (38.78%)	
Margin			0.721
Clear	27 (65.85%)	34 (69.39%)	
Unclear	14 (34.15%)	15 (30.61%)	
Morphology			0.476
Regular	17 (41.16%)	24 (48.98%)	
Irregular	24 (58.54%)	25 (51.02%)	

[a]Data are presented as median (range)

[b]Data are means±standard deviations, with ranges in parentheses

*Statistically significant at $P <$ 0.05

Unless otherwise indicated, data are number of lesions, with percentages in parentheses

ICC Intrahepatic Cholangiocarcinoma, *P-HCC* poorly differentiated Hepatocellular Carcinoma, *BMI* Body mass index, *AFP* alpha fetoprotein, *CA*199 Carbohydrate antigen 199

Multivariate regression and LASSO regression analysis

Patient features with $P < 0.05$ in the univariate analysis were incorporated into the multivariate logistic regression model, and the independent influencing factors were determined via ENTER, as shown in Table 3. Meanwhile, LASSO regression was applied to solve the multicollinearity relationships of all features, and the coefficient of each variable was generated (Fig. 2). We screened out four variables with the optimal lambda ($\lambda = 0.1095613$). These variables were enhancement level in the KP (0.9029231), hepatitis (− 0.3887257), AFP level (> 20 μg/L) (− 0.6085682), washout time (≤ 45 s) (0.6220081), and multivariate logistic regression analysis with $P < 0.05$.

Development and validation of the nomogram

The following model was constructed based on the independent variables selected by multivariate regression analysis and LASSO regression: Predicted value = − 5.399 + 2.404Age − 1.023Hepatitis-1.540AFP+1.452washout time +2.801 Enhancement level in the KP (age> 51 y, value 1; hepatitis, value 1; AFP> 20 μg/L, value 1; washout time≤ 45s, value 1; enhancement level in the KP (defect), value 1).

Therefore, we constructed a nomogram (Fig. 3). The cutoff value of the nomogram was 0.430. When it was more significant than 0.430, the diagnosis was ICC (Fig. 4), and vice versa, the diagnosis was P-HCC (Fig. 5). Using this nomogram, the C-statistic was 0.930 (95% CI: 0.856-0.973) (Table 4).

The Hosmer-Lemeshow goodness-of-fit test showed good fit in the cohort ($P = 0.437$). The calibration curve (Fig. 6a) showed that the predicted incidence was more consistent with the actual incidence of ICC, and 400 times repeated 3-fold cross-validation revealed good discrimination with a mean AUC of 0.851. Decision curve analysis showed that the nomogram could increase the net benefit to the patient (Fig. 6b).

Sonographers' Diagnosis and CEUS LI-RADS Categories

According to the sonographers' diagnosis given by each center, only 17 ICCs were correctly diagnosed, 14 ICCs were diagnosed as HCC, 8 ICCs were diagnosed as metastasis, and 2 ICCs were diagnosed as benign lesions. However, among 49 P-HCCs, 48 P-HCCs were correctly diagnosed as HCC.

According to CEUS LI-RADS, 10 (24.39%) ICCs were finally classified as non-LI-M, and 17 (34.69%) P-HCCs were classified as LI-M (Supplement Table 3). The classification of LI-M according to the CEUS LI-RADS criteria by two sonographers had a kappa-value of 0.608.

The nomogram was compared with the above methods, and the validity of the nomogram was better than that of the sonographers' diagnosis and CEUS LI-RADS categories ($P < 0.001$), as shown in Table 4. The diagnostic performance of ICC is shown in Fig. 7.

Table 2 SCEUS features in ICC and P-HCC

Features	ICC (n = 41)	P-HCC (n = 49)	P
Enhancement level in the AP			0.09
Hyper-enhancement	34 (82.93%)	46 (93.88%)	
Iso-enhancement	2 (4.88%)	2 (4.08%)	
Hypo-enhancement	5 (12.19%)	1 (2.04%)	
Rim enhancement	7 (17.07%)	4 (8.16%)	0.199
Washout time			< 0.001*
≤ 45 s	32 (78.05%)	12 (24.49%)	
> 45 s	9 (21.95%)	37 (75.51%)	
Washout time			< 0.001*
< 60 s	31 (75.61%)	17 (34.69%)	
≥ 60 s	10 (24.39%)	32 (65.31%)	
Enhancement level in the KP			< 0.001*
Hypo-enhancement	8 (19.51%)	37 (75.51%)	
Defect	33 (80.49%)	12 (24.49%)	
Margin in the KP			0.713
Clear	21 (51.22%)	27 (55.10%)	
Unclear	20 (48.78%)	22 (44.90%)	
Morphology in the KP			0.598
Regular	19 (46.34%)	20 (40.82%)	
Irregular	22 (53.66%)	29 (59.18%)	

*Statistically significant at $P < 0.05$

Data are number of lesions, with percentages in parentheses

SCEUS Sonazoid contrast-enhanced ultrasound, *ICC* Intrahepatic Cholangiocarcinoma, *P-HCC* poorly differentiated Hepatocellular Carcinoma, *AP* Arterial phase, *KP* Kupffer phase

Discussion

In this study, we report the ability to differentiate ICC from P-HCC by developing a nomogram model that uses clinical and SCEUS features. Compared to sonographers' diagnosis and CEUS LI-RADS categories, our model showed a higher sensitivity and improved accuracy in identifying ICC from P-HCC with atypical vascular phase; it demonstrated higher predictive performance (AUC = 0.930); and the accuracy rate reached 88.9%. Notably, the innovation was that the model was based on clinical and SCEUS features for non-invasive differentiation of difficult-to-identify lesions prior to treatment.

Sonazoid® can be used to detect the presence of Kupffer cells, since these microbubbles are easily taken up by Kupffer cells [24].Therefore, it has an additional Kupffer phase (KP), which starts approximately 10 min postinjection, when the microbubbles have been eliminated from the blood pool [25, 26]. Previous studies [27, 28] have demonstrated that the enhancement level in KP varies in

Table 3 Univariate and Multivariate Analysis of clinical and SCEUS features

	Univariate analysis			Multivariate analysis		
	OR	95% CI	P	OR	95% CI	P
Age (> 51years)	5.961	2.217–16.031	< 0.001	10.994	1.691–71.470	0.012
Sex (Male)	0.275	0.087–0.862	0.027			
Hepatitis (no)	0.089	0.029–0.270	< 0.001			
AFP> 20μg/L	0.116	0.045–0.302	< 0.001	0.110	0.020–0.608	0.011
CA199> 37μ/mL	2.637	1.092–6.369	0.029			
Gray-scale Echogenicity	2.820	1.038–7.663	0.042			
Washout time (≤ 45 s)	10.963	4.093–29.366	< 0.001			
Enhancement level in the KP	12.719	4.631–34.928	< 0.001	10.726	1.471–78.204	0.019
Gray value ratio (> 2.24)	16.889	4.582–62.249	< 0.001			

Parameters with a P-value of < 0.05 in univariable analysis are included in the multivariable analysis

OR Odds ratio, *CI* confidence interval, *AFP* alpha fetoprotein, *CA199* Carbohydrate antigen 199, *KP* Kupffer phase

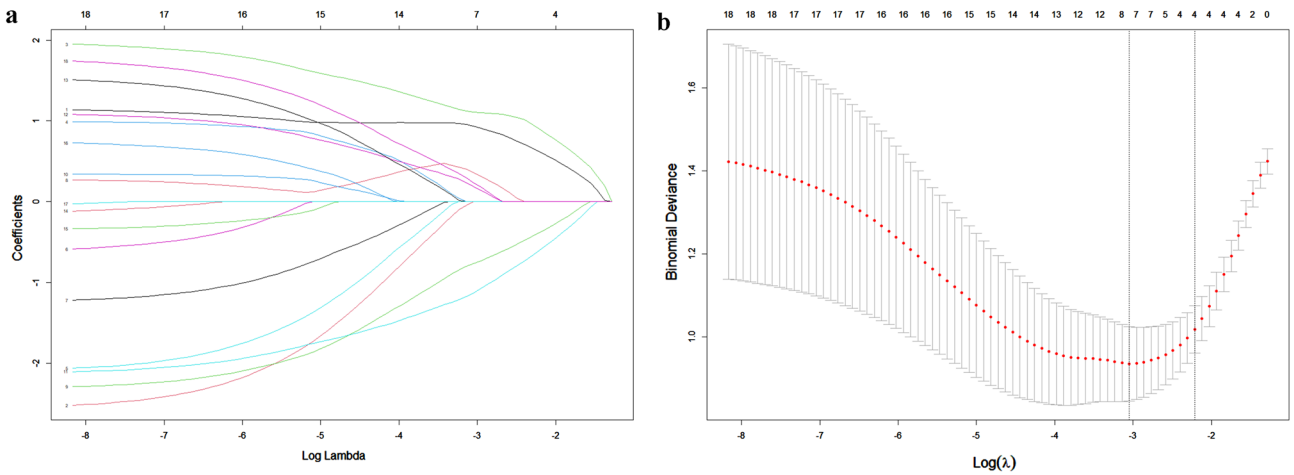

Fig. 2 Clinical and ultrasound feature selection with least absolute shrinkage and selection operator (LASSO) regression. A coefficient profile plot was produced against the log(lambda) sequence (**a**). Four variables with nonzero coefficients were selected by the optimal lambda. By verifying the optimal parameter (lambda) in the LASSO model, the partial likelihood deviance (binomial deviance) curve was plotted versus log(lambda), and dotted vertical lines were drawn based on 1 standard error criterion (**b**)

benign and malignant lesions and could differentiate HCC grades. Kupffer cells rarely or almost never exist in malignant lesions, making the contrast intensity different between lesions during the Kupffer phase. Malignant lesions showed hypo-enhancement in KP, while non-HCC malignant lesions were more likely to show a cavity-like appearance in the KP with approximately no enhancement [26, 29]. In 2020, Sugimoto, K. [30] proposed a modified CEUS LI-RADS

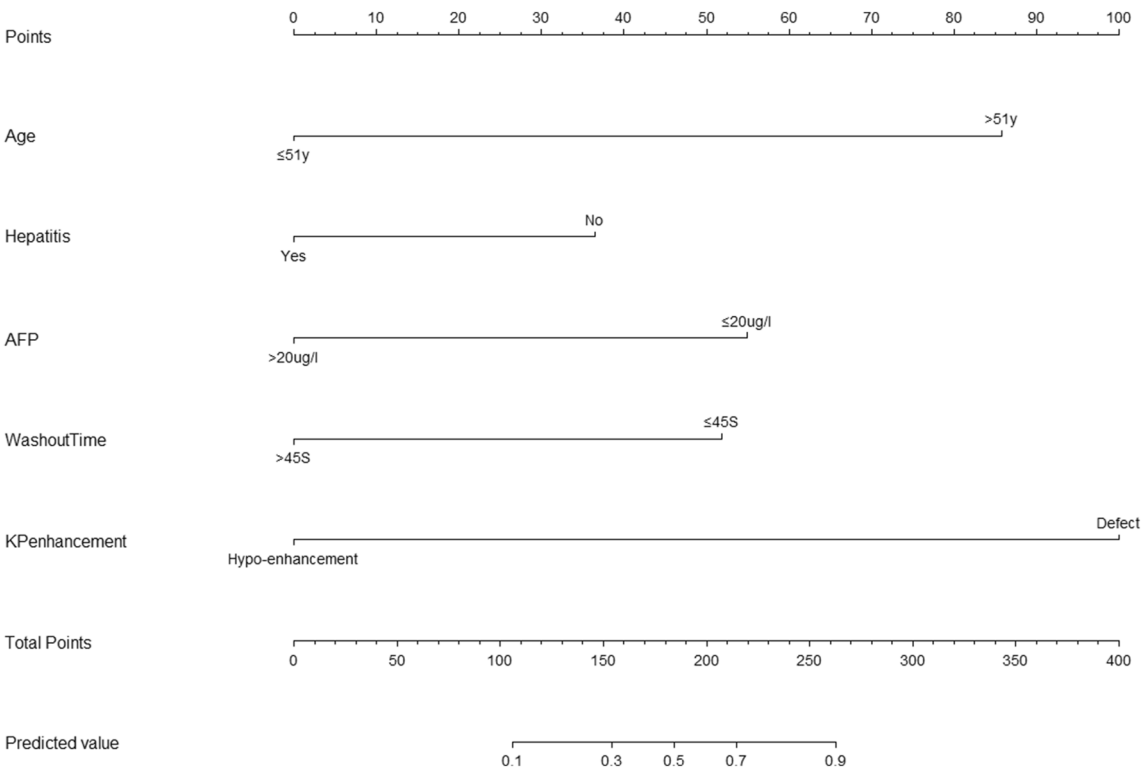

Fig. 3 A nomogram was developed with predictors including age, hepatitis, AFP level, washout time, and KP enhancement level. Draw a vertical straight line from the variable value to the axis labeled "Points". Then calculate five variables' points. The total points on the bottom scales that correspond to the predicted value are shown

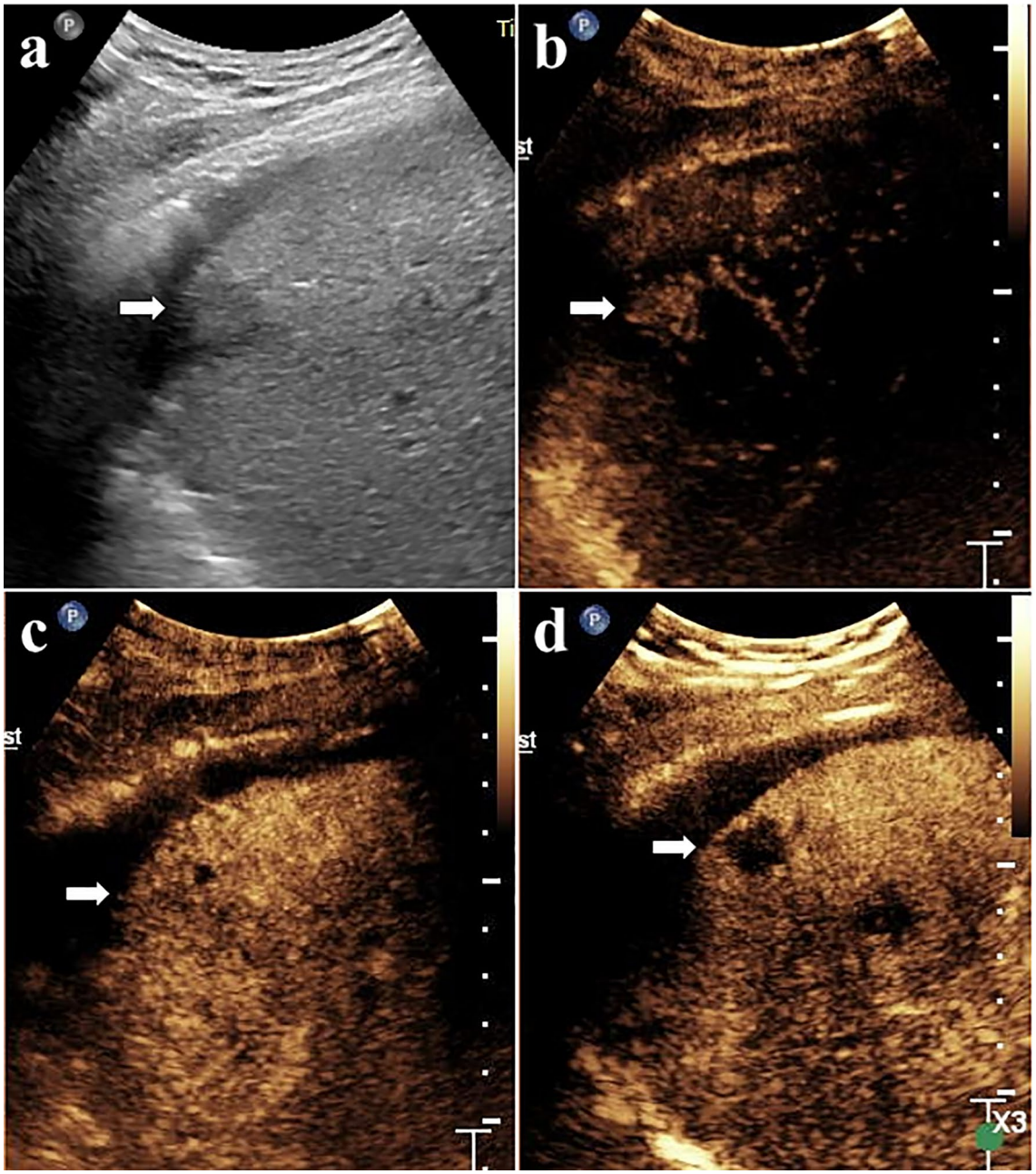

Fig. 4 ICC in a 60-year-old patient. **a** Gray-scale ultrasound showed a hypoechoic nodule (arrow) in liver S8, with a maximum diameter of approximately 2.0 cm. The edge was blurred, and the morphology was irregular. **b** Hyper-enhancement (arrow) in the AP (30 s) after injection of the Sonazoid contrast agent. **c** At 108 s after injection, the lesion began to wash out (arrow). **d** After 10 minutes (Kupffer phase), the lesion (arrow) showed marked washout. According to the LI-RADS CUES, the lesion was classified as LI-5. According to the nomogram, the risk value was 0.830(> 0.430); this lesion was predicated to be ICC. The pathological diagnosis was ICC

for Sonazoid, which included the enhancement level in the KP and improved the accuracy of diagnosing focal liver lesions. However, the KP enhancement level was not further classified into the LI-5 and LI-M classification criteria. Our study demonstrated that the enhancement level (hypo-enhancement /defect) in the KP, as subjectively assessed by sonographers, was an independent risk factor that could affect the differential diagnosis of P-HCC and ICC, OR: 10.726 (95% CI 1.471-78.204), P=0.019. In our

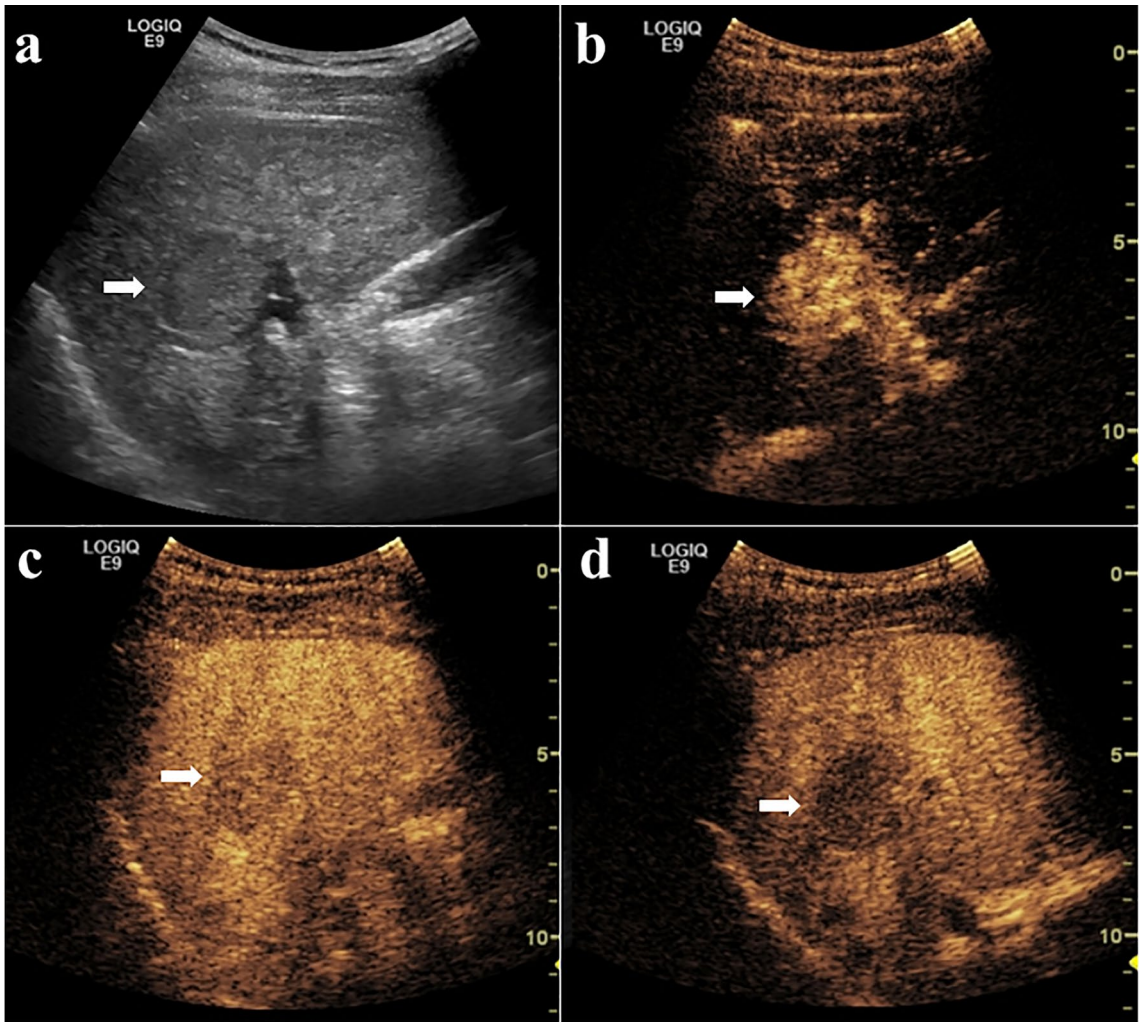

Fig. 5 P-HCC in a 33-year-old patient. **a** Gray-scale ultrasound showed a hypoechoic lesion(arrow) at the junction of liver S8 and S5, with a maximum diameter of approximately 3.3cm.The edge was clear and the morphology was regular. **b** Hyper-enhancement (arrow) in the early AP (16 s) after injection of the Sonazoid contrast agent. **c** At 48 s after injection, the lesion began to wash out (arrow). **d** After 10 minutes (Kupffer phase), the lesion (arrow) shows mild washout. According to the LI-RADS CUES, the lesion was classified as LI-M. According to the nomogram, the risk value was 0.024(< 0.430); this lesion was predicated to be P-HCC. The pathological diagnosis was P-HCC

Table 4 Diagnostic efficacy of different methods

	AUC (95% CI)	Sensitivity (%)	Specificity (%)	PPV (%)	NPV (%)
Sonographers	0.697 (0.591, 0.790)	41.46	97.96	94.44	66.67
CEUS LI-RADS	0.705 (0.599, 0.796)	75.61	65.31	64.58	76.19
Nomogram	0.930 (0.856, 0.973)	92.68	85.71	84.44	93.33

95% confidence intervals are shown in parentheses

AUC Area under the receiver operating characteristic, *CI* confidence interval, *PPV* Positive predictive value, *NPV* Negative predictive value

cohort, 33 (80.49%) ICCs exhibit KP defects, which could initially distinguish them from P-HCC, with an AUC of 0.780 (95% CI 0.681-0.879). This finding was confirmed in the gray-scale analysis using ImageJ software (Supplement Table 2), which showed a significant difference in the mean gray value of ICC and P-HCC in the KP ($P = 0.004$).

Several studies have reported that certain ultrasound features, such as bile duct dilatation or cholangiolithiasis,

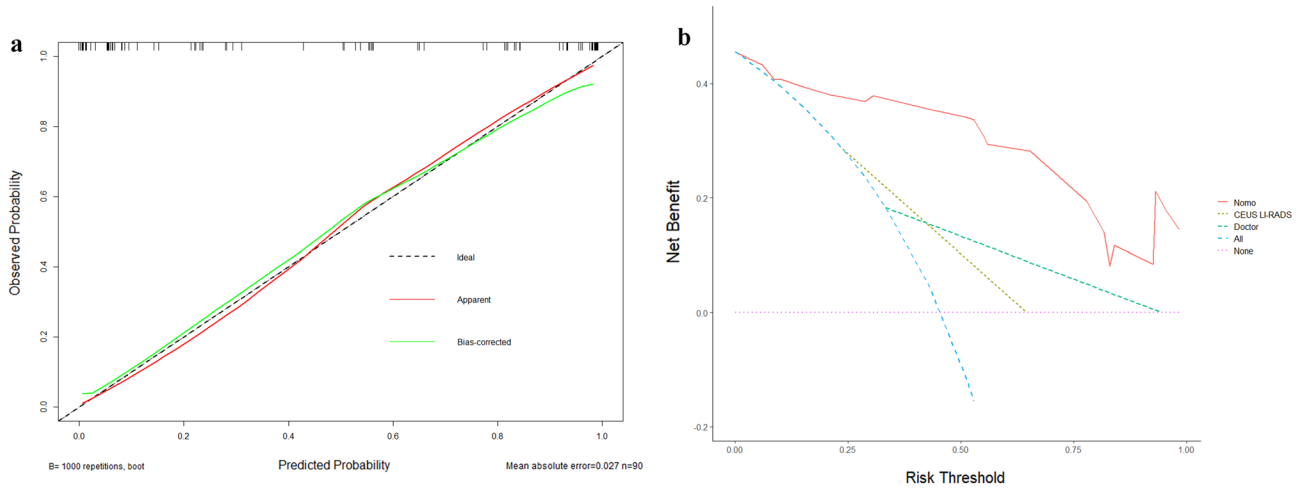

Fig. 6 Calibration curves (**a**) of the nomogram prediction. The y-axis indicates the actual diagnosed ICC. The x-axis indicates the predicted risk of ICC. The diagonal dotted line indicates a perfect prediction by an ideal model. The solid line represents the performance of the cohort, which indicates that a closer fit to the diagonal dotted line represents a better prediction. Decision curve analysis (**b**) showed that it would be more accurate to use this nomogram to predict the risk of ICC. The quantified net benefits can be measured at different threshold probabilities. The y-axis denotes the standardized net benefit, and the x-axis indicated the risk threshold probabilities. The orange line represents the nomogram, the blue dotted line represents the condition that all patients have ICC, and the pink dotted line represents the condition that none have ICC

irregular rim enhancement, and early washout time, were found to have diagnostic value for ICC [31, 32]. However, in our study, there were no significant differences in gray-scale ultrasound features, arterial phase enhancement patterns, and rim enhancement between P-HCC and ICC, which was partially inconsistent with Yuan M's study [32]. This may be attributed to the different patients enrolled. Furthermore, it is noteworthy that some ICCs do not exhibit typical signs such as bile duct dilatation, and these patients may have a history of hepatitis, leading to subjective misclassification of them as HCCs by sonographers. However, sonographers could accurately diagnose the ICC with typical CEUS features, resulting in a high specificity of 97.96%.

According to the vascular phase (< 120 s), the CEUS LI-RADS categories was evaluated, and the sensitivity and specificity of classifying ICC as LI-M were 75.6% and 65.3%, respectively. These were slightly lower than those reported by Zheng et al. [33], who found the sensitivity and specificity to classify the ICC as LI-M to be 89% and 88%, respectively. Our analysis revealed that some P-HCCs were difficult to distinguish from ICCs in the vascular phase, with high enhancement in the arterial phase and the early washout time (< 60 s), which may lead to misclassification by the CEUS LI-RADS categories. We also found that P-HCC and ICC could be better discriminated ($P < 0.001$) when the early washout time was defined as 45 seconds.

Given the similarity of the vascular phase enhancement patterns between some P-HCCs and ICCs, the accuracy of sonographers' diagnosis may be compromised. To address this issue, we developed an ICC-predicted nomogram

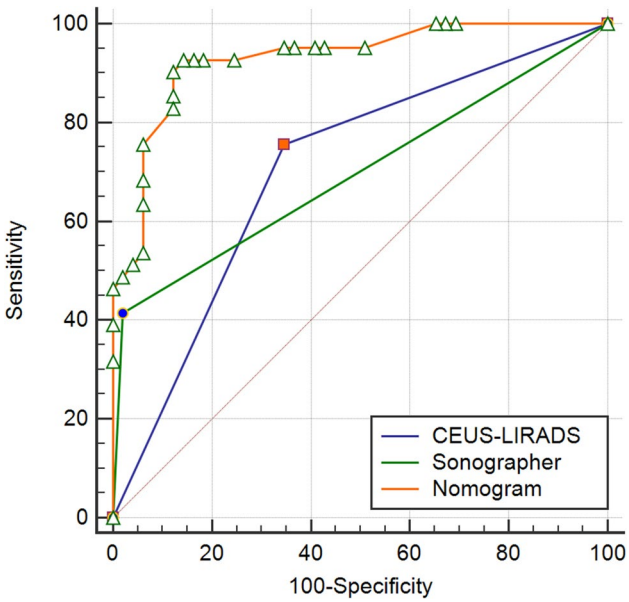

Fig. 7 Discrimination of the nomogram was evaluated by the ROC curve. The y-axis indicates the true-positive rate of the risk prediction. The x-axis indicates the false-positive rate of the risk prediction. The orange line represents the performance of the nomogram. AUC=0.930 which is equal to the c-statistic

that is comprised of five risk factors. The AUC of the nomogram was 0.930, which was higher than the sonographers' diagnosis and CEUS LI-RADS categories. The 400 times repeated 3-fold cross-validation showed that the mean AUC was 0.851, which indicates a relatively

reliable result. This approach may provide a new diagnostic method for tumors that are challenging to differentiate by gray-scale ultrasound and SonoVue CEUS. With the ability to diagnose more ICC, more appropriate treatment options can be further selected to improve the overall prognosis.

Nevertheless, our study has some limitations. While it is a multicenter study, the number of cases of P-HCC and ICC was small. Further validation is necessary to indicate the model's general applicability and improve it if necessary. Additionally, some tumor specimens were obtained by biopsy. Due to the heterogeneity of tumors, combined hepatocellular carcinoma may not be ruled out. But owing to its low incidence, it was included in this article.

Conclusion

This study found that clinical indicators such as age, hepatitis, and AFP were helpful in the diagnosis of ICC. The enhancement level in the KP and early washout time ($\leq$ 45 s) were identified as independent risk factors for differentiating ICC from P-HCC. The nomogram constructed based on SCEUS and clinical features has the potential to noninvasively diagnose the ICC before surgery and may provide some support for clinical treatment decision-making.

Supplementary Information The online version contains supplementary material available at https://doi.org/10.1007/s00261-023-03993-z.

Author contributions All authors contributed to the study conception and design. The first draft of the manuscript was written by SW and all authors commented on the previous versions of the manuscript. All authors read and approved the final manuscript.

Funding This study was funded by the National Scientific Foundation Committee of China (Grants 82172027).

Declarations

Competing interest The authors have no relevant financial or non-financial interests to disclose.

Ethical approval All procedures performed in studies involving human participants were in accordance with the ethical standards of the institutional and/or national research committee and with the 1964 Helsinki Declaration and its later amendments or comparable ethical standards. This study was approved by the Institutional Review Boards at each center (S2020-300-01)

Consent to participate Informed consent was obtained from all individual participants included in the study.

References

1. Sung H, Ferlay J, Siegel RL, Laversanne M, Soerjomataram I, Jemal A, Bray F. Global Cancer Statistics 2020: GLOBOCAN Estimates of Incidence and Mortality Worldwide for 36 Cancers in 185 Countries. CA Cancer J Clin 2021;71:209-249.
2. Sahu SK, Chawla YK, Dhiman RK, Singh V, Duseja A, Taneja S, Kalra N, et al. Rupture of Hepatocellular Carcinoma: A Review of Literature. J Clin Exp Hepatol 2019;9:245-256.
3. European Association for the Study of the Liver Ea, easloffice easloffice eu, European Association for the Study of the L. EASL Clinical Practice Guidelines: Management of hepatocellular carcinoma. J Hepatol 2018;69:182-236.
4. Kudo M, Trevisani F, Abou-Alfa GK, Rimassa L. Hepatocellular Carcinoma: Therapeutic Guidelines and Medical Treatment. Liver Cancer 2016;6:16-26.
5. Wang K, Zhang H, Xia Y, Liu J, Shen F. Surgical options for intrahepatic cholangiocarcinoma. Hepatobiliary Surg Nutr 2017;6:79-90.
6. Patrone R, Izzo F, Palaia R, Granata V, Nasti G, Ottaiano A, Pasta G, et al. Minimally invasive surgical treatment of intrahepatic cholangiocarcinoma: A systematic review. World J Gastrointest Oncol 2021;13:2203-2215.
7. Galassi M, Iavarone M, Rossi S, Bota S, Vavassori S, Rosa L, Leoni S, et al. Patterns of appearance and risk of misdiagnosis of intrahepatic cholangiocarcinoma in cirrhosis at contrast enhanced ultrasound. Liver Int 2013;33:771-779.
8. Little JM, Richardson A, Tait N. Hepatic dystychoma: a five year experience. HPB Surg 1991;4:291-297.
9. Boozari B, Soudah B, Rifai K, Schneidewind S, Vogel A, Hecker H, Hahn A, et al. Grading of hypervascular hepatocellular carcinoma using late phase of contrast enhanced sonography - a prospective study. Dig Liver Dis 2011;43:484-490.
10. Jang HJ, Kim TK, Burns PN, Wilson SR. Enhancement patterns of hepatocellular carcinoma at contrast-enhanced US: comparison with histologic differentiation. Radiology 2007;244:898-906.
11. Hatanaka K, Kudo M, Minami Y, Maekawa K. Sonazoid-enhanced ultrasonography for diagnosis of hepatic malignancies: comparison with contrast-enhanced CT. Oncology 2008;75 Suppl 1:42-47.
12. Sugimoto K, Moriyasu F, Saito K, Taira J, Saguchi T, Yoshimura N, Oshiro H, et al. Comparison of Kupffer-phase Sonazoid-enhanced sonography and hepatobiliary-phase gadoxetic acid-enhanced magnetic resonance imaging of hepatocellular carcinoma and correlation with histologic grading. J Ultrasound Med 2012;31:529-538.
13. Li C, Xu J, Liu Y, Wu M, Dai W, Song J, Wang H. Kupffer Phase Radiomics Signature in Sonazoid-Enhanced Ultrasound is an Independent and Effective Predictor of the Pathologic Grade of Hepatocellular Carcinoma. J Oncol 2022;2022:6123242.
14. Dietrich CF, Nolsoe CP, Barr RG, Berzigotti A, Burns PN, Cantisani V, Chammas MC, et al. Guidelines and Good Clinical Practice Recommendations for Contrast-Enhanced Ultrasound (CEUS) in the Liver-Update 2020 WFUMB in Cooperation with EFSUMB, AFSUMB, AIUM, and FLAUS. Ultrasound Med Biol 2020;46:2579-2604.
15. Washington MK, Goldberg RM, Chang GJ, Limburg P, Lam AK, Salto-Tellez M, Arends MJ, et al. Diagnosis of digestive system tumours. Int J Cancer 2021;148:1040-1050.
16. Lee JY, Minami Y, Choi BI, Lee WJ, Chou YH, Jeong WK, Park MS, et al. The AFSUMB Consensus Statements and Recommendations for the Clinical Practice of Contrast-Enhanced Ultrasound using Sonazoid. Ultrasonography 2020;39:191-220.

17. Radiology ACo. CEUS LI-RADS version 2017. In: American College of Radiology; 2017.
18. Cannella R, Furlan A. Mosaic architecture of hepatocellular carcinoma. Abdom Radiol (NY) 2018;43:1847-1848.
19. Dietrich CF, Dong Y, Kono Y, Caraiani C, Sirlin CB, Cui XW, Tang A. LI-RADS ancillary features on contrast-enhanced ultrasonography. Ultrasonography 2020;39:221-228.
20. Kang HJ, Kim JH, Yoo J, Han JK. Diagnostic criteria of perfluorobutane-enhanced ultrasonography for diagnosing hepatocellular carcinoma in high-risk individuals: how is late washout determined? Ultrasonography 2022;41:530-542.
21. Li L, Zheng W, Wang J, Han J, Guo Z, Hu Y, Li X, et al. Contrast-Enhanced Ultrasound Using Perfluorobutane: Impact of Proposed Modified LI-RADS Criteria on Hepatocellular Carcinoma Detection. AJR Am J Roentgenol 2022;219:434-443.
22. Huang Z, Zhou P, Li S, Li K. Evaluation of contrast-enhanced ultrasound LI-RADS version 2017: application on 271 liver nodules in individuals with non-alcoholic steatohepatitis. Eur Radiol 2022.
23. Matsumoto N, Ogawa M, Takayasu K, Hirayama M, Miura T, Shiozawa K, Abe M, et al. Quantitative sonographic image analysis for hepatic nodules: a pilot study. J Med Ultrason (2001) 2015;42:505-512.
24. Yanagisawa K, Moriyasu F, Miyahara T, Yuki M, Iijima H. Phagocytosis of ultrasound contrast agent microbubbles by Kupffer cells. Ultrasound Med Biol 2007;33:318-325.
25. Shunichi S, Hiroko I, Fuminori M, Waki H. Definition of contrast enhancement phases of the liver using a perfluoro-based microbubble agent, perflubutane microbubbles. Ultrasound Med Biol 2009;35:1819-1827.
26. Barr RG, Huang P, Luo Y, Xie X, Zheng R, Yan K, Jing X, et al. Contrast-enhanced ultrasound imaging of the liver: a review of the clinical evidence for SonoVue and Sonazoid. Abdom Radiol (NY) 2020;45:3779-3788.
27. Korenaga K, Korenaga M, Furukawa M, Yamasaki T, Sakaida I. Usefulness of Sonazoid contrast-enhanced ultrasonography for hepatocellular carcinoma: comparison with pathological diagnosis and superparamagnetic iron oxide magnetic resonance images. J Gastroenterol 2009;44:733-741.
28. Zou RH, Lin QG, Huang W, Li XL, Cao Y, Zhang J, Zhou JH, et al. Quantitative Contrast-Enhanced Ultrasonic Imaging Reflects Microvascularization in Hepatocellular Carcinoma and Prognosis after Resection. Ultrasound Med Biol 2015;41:2621-2630.
29. Lv K, Zhai H, Jiang Y, Liang P, Xu HX, Du L, Chou YH, et al. Prospective assessment of diagnostic efficacy and safety of Sonazoid(TM) and SonoVue((R)) ultrasound contrast agents in patients with focal liver lesions. Abdom Radiol (NY) 2021;46:4647-4659.
30. Sugimoto K, Kakegawa T, Takahashi H, Tomita Y, Abe M, Yoshimasu Y, Takeuchi H, et al. Usefulness of Modified CEUS LI-RADS for the Diagnosis of Hepatocellular Carcinoma Using Sonazoid. Diagnostics (Basel) 2020;10.
31. Guo HL, Zheng X, Cheng MQ, Zeng D, Huang H, Xie XY, Lu MD, et al. Contrast-Enhanced Ultrasound for Differentiation Between Poorly Differentiated Hepatocellular Carcinoma and Intrahepatic Cholangiocarcinoma. J Ultrasound Med 2022;41:1213-1225.
32. Yuan M, Li R, Zhang Y, Yang L, Zhang X, Tang C, Guo D. Enhancement Patterns of Intrahepatic Cholangiocarcinoma on Contrast-Enhanced Ultrasound: Correlation with Clinicopathologic Findings and Prognosis. Ultrasound Med Biol 2019;45:26-34.
33. Zheng W, Li Q, Zou XB, Wang JW, Han F, Li F, Huang LS, et al. Evaluation of Contrast-enhanced US LI-RADS version 2017: Application on 2020 Liver Nodules in Patients with Hepatitis B Infection. Radiology 2020;294:299-307.

Authors and Affiliations

Shuo Wang[1,2] · Jundong Yao[1,3] · Kaiyan Li[4] · Hong Yang[5] · Shichun Lu[6] · Guangzhi He[7] · Wei Wu[8] · Wen Cheng[9] · Tianan Jiang[10] · Hong Ding[11] · Xiang Jing[12] · Yuanyuan Yan[13] · Fangyi Liu[14] · Jie Yu[14] · Zhiyu Han[14] · Zhigang Cheng[14] · Shuilian Tan[14] · Xin Li[14] · Jianping Dou[14] · Yunlin Li[1] · Erpeng Qi[1] · Yiqiong Zhang[1] · Ping Liang[14] · Xiaoling Yu[1]

✉ Ping Liang
liangping301@hotmail.com

✉ Xiaoling Yu
dyuxl301@aliyun.com

Shuo Wang
shea1214@163.com

Jundong Yao
yjd2313@outlook.com

Kaiyan Li
Liky20006@126.com

Hong Yang
yanghong@gxmu.edu.cn

Shichun Lu
lsc620213@aliyun.com

Guangzhi He
810080705@qq.com

Wei Wu
wuvei@163.com

Wen Cheng
chengwenhmu@126.com

Tianan Jiang
tiananjiang@zju.edu.cn

Hong Ding
ding_hong@fudan.edu.cn

Xiang Jing
dr.jingxiang@aliyun.com

Yuanyuan Yan
779744399@qq.com

Fangyi Liu
fangyi0317@163.com

Jie Yu
jiemi301@163.com

Zhiyu Han
hanzhiyu301@hotmail.com

Zhigang Cheng
13691367317@163.com

Shuilian Tan
tanshuilian301@163.com

Xin Li
lixin301@hotmail.com

Jianping Dou
jianpingdou2006@163.com

Yunlin Li
liyunlin301@163.com

Erpeng Qi
hellosheldon@126.com

Yiqiong Zhang
17211220117@fudan.edu.cn

[1] Department of Interventional Ultrasound, First Medical Center of Chinese PLA General Hospital, No.28 Fuxing Road, Beijing 100853, China

[2] Chinese PLA Medical School, Beijing 100853, China

[3] Department of Ultrasound, The First Affiliated Hospital of Henan University of Science and Technology, Luoyang 471000, China

[4] Department of Ultrasound, Affiliated Tongji Hospital of Tongji Medical College, Huazhong University of Science and Technology, Wuhan 430030, China

[5] Department of Ultrasound, The First Affiliated Hospital of Guangxi medical University, Nanning 530021, China

[6] Department of Hepatobiliary Surgery, First Medical Center of Chinese PLA General Hospital, Beijing 100853, China

[7] Department of Ultrasound, University of Chinese Academy of Sciences Shenzhen Hospital, Guangming District, Shenzhen 518000, China

[8] Department of Ultrasound, Peking University Cancer Hospital & Institute, Beijing 100142, China

[9] Department of Ultrasonography, Harbin Medical University Cancer Hospital, Harbin 150000, China

[10] Department of Ultrasound Medicine, The First Affiliated Hospital, Zhejiang University School of Medicine, Hangzhou 310000, China

[11] Department of Ultrasound, Huashan Hospital, Fudan University, Shanghai 200040, China

[12] Department of Ultrasound, Tianjin Third Central Hospital, Tianjin 300170, China

[13] Department of Ultrasound, Zhengzhou Central Hospital Affiliated to Zhengzhou University, Henan 450007, China

[14] Department of Interventional Ultrasound, Fifth Medical Center of ChinesePLA General Hospital, No.28 Fuxing Road, Beijing 100853, China